

# DYNAMIC NOVEL VIEW SYNTHESIS IN HIGH DYNAMIC RANGE

Kaixuan Zhang<sup>1</sup> Zhipeng Xiong<sup>1</sup> Minxian Li<sup>1\*</sup> Mingwu Ren<sup>1</sup>

Jiankang Deng<sup>2</sup> Xiatian Zhu<sup>3</sup>

<sup>1</sup>Nanjing University of Science and Technology    <sup>2</sup>Imperial College London    <sup>3</sup>University of Surrey

## ABSTRACT

High Dynamic Range Novel View Synthesis (HDR NVS) seeks to learn an HDR 3D model from Low Dynamic Range (LDR) training images captured under conventional imaging conditions. Current methods primarily focus on static scenes, implicitly assuming all scene elements remain stationary and non-living. However, real-world scenarios frequently feature dynamic elements, such as moving objects, varying lighting conditions, and other temporal events, thereby presenting a significantly more challenging scenario. To address this gap, we propose a more realistic problem named HDR Dynamic Novel View Synthesis (HDR DNVS), where the additional dimension “Dynamic” emphasizes the necessity of jointly modeling temporal radiance variations alongside sophisticated 3D translation between LDR and HDR. To tackle this complex, intertwined challenge, we introduce HDR-4DGS, a Gaussian Splatting-based architecture featured with an innovative dynamic tone-mapping module that explicitly connects HDR and LDR domains, maintaining temporal radiance coherence by dynamically adapting tone-mapping functions according to the evolving radiance distributions across the temporal dimension. As a result, HDR-4DGS achieves both temporal radiance consistency and spatially accurate color translation, enabling photorealistic HDR renderings from arbitrary viewpoints and time instances. Extensive experiments demonstrate that HDR-4DGS surpasses existing state-of-the-art methods in both quantitative performance and visual fidelity. Source code will be released.

## 1 INTRODUCTION

Recent years have seen remarkable progress in Novel View Synthesis (NVS), which reconstructs 3D scene representations from multi-view images to enable photorealistic rendering from arbitrary viewpoints. These advances have fueled applications in gaming (Niedermayr et al., 2024), AR / VR (Zhou et al., 2018), and autonomous driving (Wang et al., 2024a). However, most existing NVS methods (Gao et al., 2022; Wu et al., 2024c) operate under two limiting assumptions: static scenes and low dynamic range inputs. These constraints significantly hinder their applicability in real-world environments, which often exhibit complex motion, time-varying illumination, and sensor-imposed luminance clipping.

Dynamic Novel View Synthesis (DNVS) extends NVS to scenes with temporal dynamics, reconstructing 4D radiance fields coherent in both space and time. Recent efforts in DNVS (Fang et al., 2022; Gao et al., 2021; Tian et al., 2023; Duan et al., 2024; Yang et al., 2024b; Cho et al., 2024) have made notable progress in modeling dynamic geometry and appearance. However, they remain restricted to LDR imagery, which fails to capture the full spectrum of scene radiance. As a result, these methods struggle under high-contrast conditions (*e.g.*, direct sunlight or low-light environments) where overexposure and underexposure lead to significant information loss. More fundamentally, LDR imaging is inherently misaligned with human visual perception, even under moderate lighting conditions. While the human eye can adapt to luminance levels spanning over ten orders of magnitude (Reinhard, 2020), typical LDR sensors cover only a narrow dynamic range.

\*Minxian Li (minxianli@njust.edu.cn) is the corresponding author with School of Computer Science and Engineering, Nanjing University of Science and Technology.

In addition, LDR images compress radiance through nonlinear camera response functions (CRFs), distorting local contrast, suppressing brightness gradients, and reducing color fidelity. These limitations not only impair perceptual quality under extreme lighting but also degrade the realism of ordinary scenes.

High Dynamic Range (HDR) imaging addresses these shortcomings by capturing a significantly broader range of luminance and color. By preserving detail in both highlights and shadows and maintaining fine-grained contrast, HDR techniques provide a closer match to the perceptual capabilities of the human visual system. Recent works in HDR NVS (Huang et al., 2022; Cai et al., 2024; Liu et al., 2025) have attempted to reconstruct HDR content from multi-exposure LDR images of calibrated sensors. However, these methods are restricted to static scenes, implicitly assuming that all elements remain fixed over time. In contrast, real-world HDR scenarios are inherently dynamic, often involving moving objects, shifting illumination, and transient phenomena. These dynamics violate the assumptions of existing HDR NVS pipelines and introduce significant challenges: non-rigid motion and temporal variation create complex spatiotemporal inconsistencies, while the lack of reliable luminance priors from sparse LDR observations leads to severe photometric ambiguities.

To bridge this gap, we introduce High Dynamic Range Dynamic Novel View Synthesis (*HDR DNVS*), a new, more practical task that seeks to reconstruct temporally coherent HDR radiance fields and dynamic geometry from sparse, time-varying LDR inputs. HDR DNVS demands the joint modeling of evolving scene structure and HDR radiance, posing both geometric and photometric challenges absent in prior static or LDR-constrained settings. To tackle this, we propose *HDR-4DGS*, a novel framework based on Gaussian Splatting (Kerbl et al., 2023) and equipped with a biologically inspired dynamic tone-mapping module. Drawing inspiration from human visual adaptation (Clifford et al., 2007), where retinal photoreceptors dynamically adjust to ambient brightness, HDR-4DGS includes a dynamic radiance context learner that models temporal radiance distributions. This is followed by per-channel tone-mapping functions that connect LDR representations with HDR space in a temporally adaptive and spatially accurate manner. This module explicitly bridges the LDR-HDR gap while maintaining radiance consistency and chromatic fidelity across time and space. Although conceptually straightforward, our proposed model embodies an intuitively elegant and computationally efficient design, which strategically adapts established sequential modeling techniques to address the core challenges of HDR DNVS with precision.

Our **contributions** are: (I) We formally introduce the HDR DNVS problem for the first time, which requires learning 4D HDR radiance fields with dynamic geometry and temporally coherent appearance from sparse LDR video input. (II) We propose HDR-4DGS, a novel Gaussian Splatting architecture featuring dynamic tone-mapping for adaptively bridging the LDR and HDR domains under complex spatiotemporal variations. (III) To enable rigorous quantitative evaluation of HDR DNVS methods, we introduce HDR-4D-Syn and HDR-4D-Real — two novel benchmark datasets comprising 8 high-fidelity synthetic scenes and 4 real-world captured sequences, respectively. Each scene is meticulously annotated with ground-truth HDR images, time-varying 3D geometry, and synchronized multi-view LDR observations. (IV) Extensive experiments show that HDR-4DGS achieves state-of-the-art performance in both quantitative metrics and perceptual quality on challenging dynamic scenes.

## 2 RELATED WORK

**Novel view synthesis (NVS)** has seen transformative progress via neural rendering techniques. Early multi-view geometric methods (Schonberger & Frahm, 2016; Wang et al., 2021) face limitations in handling occlusions, textureless regions, and computing efficiency (Jiang, 2023). Modern approaches leverage continuous scene representations via deep networks, such as Neural Radiance Fields (NeRF) (Mildenhall et al., 2021) and the variants (Deng et al., 2022; Roessle et al., 2022; Wei et al., 2021; Xu et al., 2022) establishing coordinate-space implicit modeling for photorealistic synthesis under spatial smoothness constraints. However, NeRF’s ray-marching paradigm suffers from high computational costs (Luo et al., 2024). In contrast, 3DGS (Kerbl et al., 2023) introduces an efficient point-based representation by parameterizing scenes as anisotropic 3D Gaussians, decoupling geometry and appearance while enabling real-time rendering with complex visual effects (*e.g.*, specular highlights). Recent advances enhance 3DGS through frequency-domain supervision (Liang et al., 2024), depth-regularized optimization (Chung et al., 2024; Kung et al., 2024; Li et al., 2024),

and memory-efficient designs (Wang et al., 2024b; Chen et al., 2024; Fan et al., 2024; Lu et al., 2024; Yang et al., 2025), achieving superior rendering quality. Nevertheless, these methods predominantly focus on static LDR scenes, limiting their applicability to real-world dynamic scenarios.

**HDR novel view synthesis (HDR NVS)** aims to reconstruct HDR scenes from multi-view LDR images. Early works like HDR-NeRF (Huang et al., 2022) extend neural radiance fields by incorporating an MLP-based tone-mapping module to bridge physical radiance and digital color spaces. To realize real-time rendering, HDR-GS (Cai et al., 2024) introduces a 3DGS framework with a neural tone-mapper that explicitly models HDR-to-LDR radiance transformations, achieving real-time HDR rendering while surpassing NeRF-based quality. Recently, GaussHDR (Liu et al., 2025) proposes to unify 3D and 2D tone mapping in 3D Gaussian Splatting to facilitate HDR rendering. However, a critical limitation of these methods is their exclusive focus on *static scenes*; none explicitly model temporal dynamics, both in spatial and color space. Consequently, they are fundamentally unable to address the core challenges posed by real-world scenarios involving time-varying geometry, non-rigid motion, or temporally evolving illumination.

Indeed, Wu et al. (2024a) preliminarily investigated dynamic HDR reconstruction from LDR sequences. Interestingly, it has never carefully evaluated the HDR output, nor verifies its performance on real-world scenes, leaving the HDR DNVS problem largely under-explored. To address these issues, we introduce a purposed benchmark by carefully re-engineering its dataset and capture a real-world dataset additionally, including LDR / HDR paired training imagery and HDR quantitative assessment. We further propose a novel HDR DNVS model, HDR-4DGS, which delivers significantly more accurate HDR renderings while operating an order of magnitude faster.

**Dynamic novel view synthesis (DNVS)** focuses on modeling dynamic scenes with time-varying geometry and radiance. The key challenge lies in capturing intrinsic spatiotemporal correlations. Building upon NeRF (Mildenhall et al., 2021), two primary approaches have emerged: *i*) implicit / explicit spatiotemporal representations decompose scenes into time-aware feature grids to learn 6D plenoptic functions (Cao & Johnson, 2023; Li et al., 2022; Fridovich-Keil et al., 2023; Wang et al., 2023), and *ii*) deformation-aware fields model motion through deformable transformations (Pumarola et al., 2021; Song et al., 2023; Abou-Chakra et al., 2024). Recent advances leverage 3DGS for dynamic rendering along two directions: *i*) deformation-based models (Wu et al., 2024b; Kratimenos et al., 2024; Bae et al., 2024; Shan et al., 2025) maintain canonical Gaussians deformed via time-varying fields, trading precise motion tracking for temporal continuity; *ii*) hyper-dimensional representations (Yang et al., 2024b; Duan et al., 2024) extend Gaussians to 4D by introducing temporal centers and spatiotemporal rotations. However, all these methods are limited to LDR outputs, and we extend this to high-fidelity HDR DNVS problem.

### 3 METHOD

**Problem** In HDR DNVS, we aim to learn a HDR 3D model  $\mathcal{F}$  for a target dynamic scene  $G$ ,  $\mathcal{F} : (t', V') \rightarrow \mathbf{I}_{t', V'}^h$ , that would render an HDR image  $\mathbf{I}_{t', V'}^h$  for any timestamp  $t'$  and viewpoint  $V'$ . To that end, we capture a set of multi-exposure LDR training images  $\mathbf{I}^l = \{\mathbf{I}_1^l, \dots, \mathbf{I}_t^l, \dots, \mathbf{I}_T^l\}$ , each  $\mathbf{I}_t^l$  associated with the exposure time  $e_t$  sampled from the choices  $E = \{e_1, \dots, e_P\}$ , and the camera viewpoint  $V_t$  selected from  $Q$  distinct viewpoints  $\mathbf{V} = \{V_1, \dots, V_Q\}$  where  $T$  denotes the total timesteps and  $P$  the number of exposure time choices. We may have *optional* access to coupled HDR training data  $\mathbf{I}^h = \{\mathbf{I}_1^h, \dots, \mathbf{I}_T^h\}$ .

#### 3.1 HDR-4DGS OVERVIEW

The HDR DNVS problem comes with additional complexity of time-evolving structures and illumination as compared to HDR NVS. To overcome that, we introduce HDR-4DGS, a Gaussian Splatting-based framework that reconstructs 4D spatiotemporal HDR radiance fields. HDR-4DGS is composed of a generic dynamic scene representation model and a novel dynamic tone-mapping mechanism. An overview is depicted in Fig. 1.

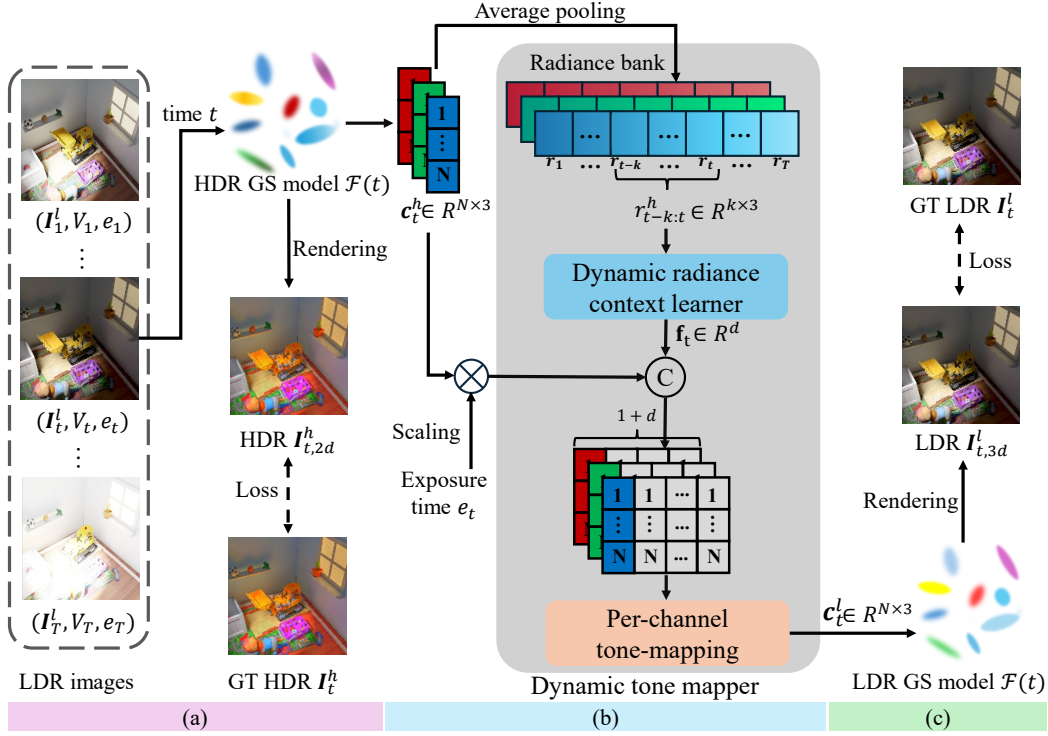


Figure 1: **Overview of HDR-4DGS.** (a) Input data and scene representation; (b) Our proposed Dynamic Tone Mapper (DTM) for temporally adaptive HDR–LDR translation; (c) Loss formulation for joint optimization of geometry, radiance, and tone mapping.  $\otimes$ : Dot product.  $\odot$ : Concatenation.

### 3.2 DYNAMIC SCENE REPRESENTATION

HDR-4DGS can integrate with existing dynamic scene representation to better capture spatiotemporal variations. Specifically, we adopt the 4D Gaussian Splatting (4DGS) framework (Yang et al., 2024a) due to its conceptual elegance and coherent formulation of dynamic scenes.

4DGS extends the formulation of 3DGS (Kerbl et al., 2023) by introducing a temporal dimension, allowing pixel observations  $\mathbf{I}$  to depend not only on spatial coordinates  $(u, v)$  in the image plane but also on an explicit timestamp  $t$ . This reformulates the original 3DGS framework as:

$$\mathbf{I}(u, v, t) = \sum_{i=1}^N p_i(t) p_i(u, v|t) \alpha_i c_i \prod_{j=1}^{i-1} (1 - p_j(t)) p_j(u, v|t) \alpha_j, \quad (1)$$

where  $p_i(t)$  is the marginal probability over time  $t$ ,  $p_i(u, v|t)$  is the conditional spatial probability given  $t$ , such that  $p_i(u, v, t) = p_i(u, v|t) \cdot p_i(t)$ , and  $N$  denotes the number of Gaussian points. Time and space are treated equally to form a unified 4D Gaussian model, where each Gaussian’s mean is denoted by  $\mu = (\mu_x, \mu_y, \mu_z, \mu_t)$ , and its covariance matrix is defined by  $\Sigma = RSS^T R^T$  with appropriately extended rotation matrix  $R$  and scaling matrix  $S$ . The marginal  $p(t)$  follows a one-dimensional Gaussian distribution:  $p(t) = \mathcal{N}(t; \mu_t, \Sigma_t)$ , where  $\mathcal{N}(\cdot)$  denotes a normal distribution.

Additionally, 4DGS incorporates a 4D extension of spherical harmonics (SH) to represent the temporal evolution of appearance. The view-dependent color  $c_i$  is modeled using a combination of 4D spherical harmonics, constructed by integrating traditional SH with Fourier series. This design enables dynamic modeling of radiance variations across time, supporting the construction of a radiance bank that facilitates HDR-LDR translation.

In our context, we extend the original color representation space of 4DGS from LDR colors to HDR colors, enabling the accurate synthesis of high-fidelity radiance fields that capture a broader range of luminance variations inherent in real-world dynamic scenes.

### 3.3 DYNAMIC TONE MAPPER

To address the challenge of maintaining temporal radiance consistency in dynamic scenes, we propose a novel dynamic tone mapper (DTM), as shown in Fig. 1(b). DTM explicitly connects the HDR and LDR domains by dynamically adapting per-channel tone-mapping functions in response to evolving temporal radiance patterns. Given a timestamp  $t$ , exposure time  $e_t$ , and current HDR color attributes  $\mathbf{c}_t^h \in \mathbb{R}^{N \times 3}$ , DTM translates HDR colors into their LDR counterparts:

$$\mathbf{c}_t^l = \text{DTM}(\mathbf{c}_t^h, e_t, t) \quad (2)$$

where  $\mathbf{c}_t^l \in \mathbb{R}^{N \times 3}$  denotes the resulting tone-mapped LDR colors.

Leveraging 4DGS’s explicit radiance modeling through 4DSH, DTM first constructs a radiance bank by storing per-timestamp mean HDR color statistics. The radiance signature  $\mathbf{r}_t^h$  for each timestamp is calculated as the average over all  $N$  Gaussian points:

$$\mathbf{r}_t^h = \frac{1}{N} \sum_{i=1}^N \mathbf{c}_{i,t}^h \in \mathbb{R}^3. \quad (3)$$

A sliding window of  $k$  previous frames collects the sequence  $\{\mathbf{r}_{t-k:t}^h\}$ , which is processed by a *Dynamic Radiance Context Learner* (DRCL) to generate a radiance context embedding:

$$\mathbf{f}_t = \text{DRCL}(\mathbf{r}_{t-k:t}^h) \in \mathbb{R}^d, \quad (4)$$

where  $d$  denotes the dimension of this context embedding. DRCL can be generally realized by any existing sequence model such as RNN (Salehinejad et al., 2017), LSTM (Staudemeyer & Morris, 2019), GRU (Cho et al., 2014) or Transformer (Vaswani et al., 2017).

To perform adaptive tone mapping, we concatenate the scaled HDR colors (converted to the logarithmic domain) with the exposure time and radiance context embedding:

$$\mathbf{c}_t^l = g_\theta([\log \mathbf{c}_t^h + \log e_t, \mathbf{f}_t]), \quad (5)$$

where  $g_\theta$  is the per-channel tone-mapping function and  $[\cdot]$  denotes concatenation. Scaling HDR colors by exposure time aligns with the principles of the CRF, which models the mapping between scene radiance and observed intensity as exposure-dependent. This normalization ensures consistent appearance modeling across varying exposure settings and facilitates stable learning. By incorporating  $\mathbf{f}_t$ , DTM enables radiance context-aware HDR-to-LDR translation, improving radiance consistency across time in dynamic scenes.

### 3.4 MODEL OPTIMIZATION

The overall objective function used to optimize HDR-4DGS is defined as:

$$\mathcal{L}_{\text{total}} = \mathcal{L}_{\text{ldr}} + \alpha \mathcal{L}_{\text{hdr}}, \quad (6)$$

where  $\mathcal{L}_{\text{ldr}}$  denotes the loss computed in the LDR domain, and  $\mathcal{L}_{\text{hdr}}$  refers to the HDR reconstruction loss. The weighting factor  $\alpha$  is set to zero if HDR ground truth is unavailable during training.

To mitigate overfitting associated with directly applying 3D tone mapping on HDR Gaussian fields (Liu et al., 2025), we adopt an extra pixel-level supervision in addition to existing ray-level supervision over the dynamic tone mapper, which introduces additional constraints to facilitate robust CRF learning:  $\mathbf{I}_{t,2d}^l = g_\theta([\log \mathbf{I}_{t,2d}^h + \log e_t, \mathbf{f}_t])$ , where  $\mathbf{I}_{t,2d}^h$  is the HDR image rasterized by the HDR Gaussian model, and  $\mathbf{I}_{t,2d}^l$  is the tone-mapped LDR image at time  $t$ . During training, we supervise both the tone-mapped LDR image  $\mathbf{I}_{t,2d}^l$  and the LDR image  $\mathbf{I}_{t,3d}^l$  rendered directly from the LDR model. This dual supervision improves the learned tone mapper’s generalization capability, as validated in our ablation (Tab. 4).

We define the image reconstruction loss as a weighted combination of  $L_1$  and D-SSIM loss (Huang et al., 2022; Nilsson & Akenine-Möller, 2020):

$$\mathcal{L}(\mathbf{I}_1, \mathbf{I}_2) = (1 - \lambda) \mathcal{L}_1(\mathbf{I}_1, \mathbf{I}_2) + \lambda \mathcal{L}_{\text{D-SSIM}}(\mathbf{I}_1, \mathbf{I}_2), \quad (7)$$

where  $\mathbf{I}_1/\mathbf{I}_2$  are paired and  $\lambda$  balances their contributions. Accordingly, the losses are defined as:

$$\mathcal{L}_{\text{ldr}} = \mathcal{L}(\mathbf{I}_{t,2d}^l, \mathbf{I}_t^l) + \mathcal{L}(\mathbf{I}_{t,3d}^l, \mathbf{I}_t^l), \quad \mathcal{L}_{\text{hdr}} = \mathcal{L}(\hat{\mathbf{I}}_{t,2d}^h, \hat{\mathbf{I}}_t^h), \quad (8)$$

where  $\mathbf{I}_t^l$  is the ground-truth LDR image. The tone-mapped HDR images  $\hat{\mathbf{I}}_{t,2d}^h$  and  $\hat{\mathbf{I}}_t^h$  are derived from the rendered HDR image  $\mathbf{I}_{t,2d}^h$  and ground-truth HDR image  $\mathbf{I}_t^h$ , respectively, using  $\mu$ -law compression:  $\hat{\mathbf{I}}^h = \frac{\log(1+\mu \cdot \text{norm}(\mathbf{I}^h))}{\log(1+\mu)}$  where  $\mu$  is a compression factor and  $\text{norm}(\cdot)$  is min-max normalization. This transformation aligns HDR and LDR domains for consistent comparison. Notably, we choose the LDR images  $\mathbf{I}_{t,3d}^l$  rasterized by Gaussian Splatting as our final LDR rendering results.

Table 1: Results on HDR-4D-Syn. \*: HDR only supervision; †: LDR+HDR supervision.

| Row | Method                                     | Supervision | PSNR $\uparrow$ | HDR SSIM $\uparrow$ | LPIPS $\downarrow$ | PSNR $\uparrow$ | LDR SSIM $\uparrow$ | LPIPS $\downarrow$ | Training time (min) | Inference speed (fps) |
|-----|--------------------------------------------|-------------|-----------------|---------------------|--------------------|-----------------|---------------------|--------------------|---------------------|-----------------------|
| 1   | HexPlane                                   | LDR         | -               | -                   | -                  | 14.20           | 0.564               | 0.551              | 28.45               | 1.60                  |
| 2   | HexPlane*                                  | HDR         | 24.89           | 0.771               | 0.377              | -               | -                   | -                  | 59.64               | 1.94                  |
| 3   | 4DGS                                       | LDR         | -               | -                   | -                  | 13.92           | 0.549               | 0.281              | 116.25              | 75.82                 |
| 4   | 4DGS*                                      | HDR         | 22.40           | 0.650               | 0.345              | -               | -                   | -                  | 44.58               | 172.61                |
| 5   | HDR-NeRF                                   | LDR         | 8.54            | 0.062               | 0.552              | 21.66           | 0.664               | 0.553              | 212.83              | 0.061                 |
| 6   | HDR-GS                                     | LDR         | 4.64            | 0.158               | 0.645              | 6.45            | 0.272               | 0.423              | <b>13.88</b>        | <b>380.38</b>         |
| 7   | HDR-GS $\dagger$                           | LDR+HDR     | 14.33           | 0.360               | 0.482              | 10.84           | 0.372               | 0.378              | 22.50               | 255.21                |
| 8   | HDR-HexPlane                               | LDR         | 14.70           | 0.649               | 0.287              | 32.59           | 0.912               | 0.145              | 37.83               | 1.61                  |
| 9   | HDR-HexPlane $\dagger$                     | LDR+HDR     | 29.30           | 0.844               | 0.223              | 31.09           | 0.896               | 0.185              | 54.31               | 1.33                  |
| 10  | <b>HDR-4DGS (Ours)</b>                     | LDR         | 25.88           | 0.865               | <b>0.076</b>       | <b>33.16</b>    | <b>0.949</b>        | <b>0.055</b>       | 69.38               | 40.80                 |
| 11  | <b>HDR-4DGS<math>\dagger</math> (Ours)</b> | LDR+HDR     | <b>30.40</b>    | <b>0.914</b>        | 0.097              | 30.69           | 0.927               | 0.097              | 76.86               | 48.63                 |

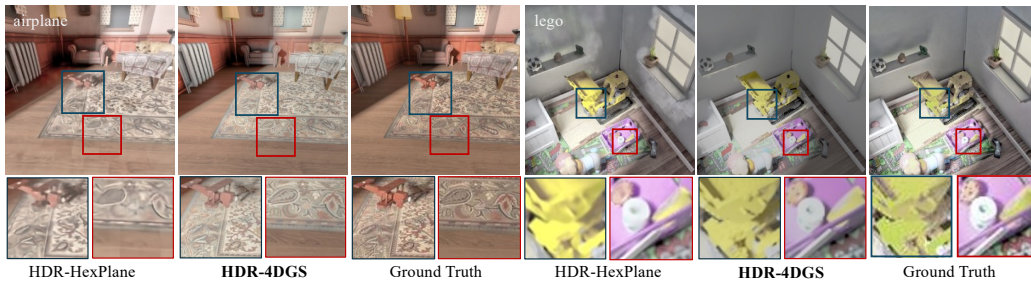


Figure 2: Visual comparison of HDR DNVS on HDR-4D-Syn.

## 4 EXPERIMENTS

**Datasets.** Due to no benchmarks for HDR DNVS, we introduce two complementary datasets: *HDR-4D-Syn* and *HDR-4D-Real*. *HDR-4D-Syn* consists of 8 synthetic dynamic scenes adapted from the dataset by Wu et al. (2024a). It features multi-exposure video sequences captured under varying exposure settings, accompanied by synchronized multi-view LDR video streams. Corresponding HDR ground truth frames are re-synthesized to ensure high-fidelity supervision and evaluation. The real-world dataset, *HDR-4D-Real*, captures 4 dynamic indoor scenes in real-world settings. Videos are recorded under three distinct exposure times using six synchronized iPhone 14 Pro devices. Ground truth HDR images are generated UltraFusion (Chen et al., 2025), ensuring realistic and high-quality HDR reconstructions. Further details are provided in Appendix A.1.

**Implementation details.** HDR-4DGS is trained with the Adam optimizer using the same parameters as 4DGS (Yang et al., 2024b). For our dynamic tone mapper, the learning rate is set to  $5 \times 10^{-4}$ , and the dimension of temporal radiance context features is set to 2. We adopt the same structure of per-channel tone-mapping functions in our dynamic tone mapper as HDR-GS (Cai et al., 2024) and GRU (Cho et al., 2014) is adopted to implement the dynamic radiance context learner by default. For equation 7,  $\lambda$  is set to 0.2, and  $\alpha$  is set to 0.6 if HDR ground truth is available.

**Evaluation metrics.** We adopt the PSNR and SSIM as quantitative metrics, LPIPS as an additional perceptual metric. Following prior works (Cai et al., 2024; Huang et al., 2022; Liu et al., 2025), we apply Photomatix Pro (HDRsoft Team, 2025) to convert HDR images into displayable LDR images for qualitative visualization and fair comparison. Furthermore, training time and inference speed (fps) are reported. *Results are averaged over all scenes.*

## 4.1 QUANTITATIVE EVALUATION

**Competitors.** We compare HDR-4DGS with latest alternatives: HexPlane (Cao & Johnson, 2023), 4DGS (Yang et al., 2024b), HDR-HexPlane (Wu et al., 2024a), HDR-NeRF (Huang et al., 2022) and HDR-GS (Cai et al., 2024). HDR-HexPlane preliminarily explores dynamic HDR synthesis by extending HexPlane with exposure conditioning and a static Sigmoid tone mapper. However, it lacks HDR supervision and omits explicit evaluation of HDR outputs, all of which have been addressed here for both fair comparison and completeness.

Table 2: Results on HDR-4D-Real. \*: HDR only supervision; †: LDR+HDR supervision.

| Row | Method                                     | Supervision | PSNR $\uparrow$ | HDR SSIM $\uparrow$ | LPIPS $\downarrow$ | PSNR $\uparrow$ | LDR SSIM $\uparrow$ | LPIPS $\downarrow$ | Training time (min) | Inference speed (fps) |
|-----|--------------------------------------------|-------------|-----------------|---------------------|--------------------|-----------------|---------------------|--------------------|---------------------|-----------------------|
| 1   | HexPlane                                   | LDR         | -               | -                   | -                  | 13.82           | 0.551               | 0.576              | <b>25.50</b>        | 0.44                  |
| 2   | HexPlane*                                  | HDR         | 32.76           | 0.893               | 0.242              | -               | -                   | -                  | 28.24               | 0.49                  |
| 3   | 4DGS                                       | LDR         | -               | -                   | -                  | 7.99            | 0.072               | 0.620              | 42.50               | <b>290.57</b>         |
| 4   | 4DGS*                                      | HDR         | 7.85            | 0.220               | 0.534              | -               | -                   | -                  | 40.75               | 307.85                |
| 5   | HDR-NeRF                                   | LDR         | 14.60           | 0.711               | 0.411              | 8.326           | 0.029               | 0.943              | 212.25              | 0.17                  |
| 6   | HDR-GS                                     | LDR         | 13.27           | 0.783               | 0.261              | 20.52           | 0.840               | 0.148              | 38.25               | 73.30                 |
| 7   | HDR-GS $\dagger$                           | LDR+HDR     | 29.40           | <b>0.936</b>        | <b>0.097</b>       | 20.85           | 0.834               | 0.182              | 56.50               | 64.88                 |
| 8   | HDR-HexPlane                               | LDR         | 9.306           | 0.672               | 0.353              | 27.44           | 0.748               | 0.353              | 36.98               | 0.35                  |
| 9   | HDR-HexPlane $\dagger$                     | LDR+HDR     | <b>33.03</b>    | 0.904               | 0.192              | 28.12           | 0.767               | 0.307              | 44.43               | 0.24                  |
| 10  | <b>HDR-4DGS (Ours)</b>                     | LDR         | 14.50           | 0.884               | 0.200              | 26.88           | 0.825               | 0.221              | 98.75               | 35.27                 |
| 11  | <b>HDR-4DGS<math>\dagger</math> (Ours)</b> | LDR+HDR     | 25.13           | 0.909               | 0.162              | <b>30.69</b>    | <b>0.927</b>        | <b>0.097</b>       | 76.86               | 48.63                 |



Figure 3: Visual comparison of HDR DNVS on HDR-4D-Real.

Although HDR-GS and HDR-NeRF were originally designed for static scenes, we adapt and train them on dynamic scenes to underscore the importance of explicit spatial modeling in dynamic HDR reconstruction. All models are evaluated with their official implementations to ensure optimal performance.

**Results.** Tab. 1 and Tab. 2 present the results for both LDR and HDR DNVS on HDR-4D-Syn and HDR-4D-Real, respectively. HDR-NeRF encounters numerical instability during training when both LDR and HDR supervision are applied simultaneously, frequently leading failed optimization. Meanwhile, 4DGS struggles to reconstruct HDR scenes on HDR-4D-Real under HDR-only supervision, as ground-truth HDR images generated via 2D methods lack multi-view consistency. We highlight the following key findings, focusing on HDR DNVS performance:

**(I) Superior HDR DNVS quality.** HDR-4DGS consistently outperforms all competing methods, including HDR-NeRF, HDR-GS, and HDR-HexPlane for HDR DNVS on HDR-4D-Syn, owing primarily to our explicit spatiotemporal HDR radiance modeling and the integration of a dynamic tone mapping mechanism that preserves temporal radiance coherence across views and exposures. In contrast, HDR-GS and HDR-NeRF rely on static tone mappers, failing to accurately bridge the HDR and LDR domains; while HDR-HexPlane achieves higher PSNR on HDR-4D-Real, we attribute this largely to the known limitations of PSNR as a metric—particularly its tendency to favor overly smooth or blurred reconstructions (Li et al., 2020), as visually demonstrated in Fig. 7. As shown in Fig. 3 and videos in the supplementary material, HDR-4DGS preserves significantly sharper spatial structure and more accurate color details than all competitors.

**(II) Effectiveness of dynamic tone mapping.** Our dynamic tone mapper plays a central role in enhancing HDR synthesis. By modeling exposure-dependent radiance dynamics with temporal context, it enables precise HDR-LDR translation and promotes stability during training and inference.



Figure 4: Comparison of HDR renderings' temporal radiance variations.

This proves essential not only for high-fidelity HDR rendering but also for generalizing under varying lighting conditions.

**(III) Training flexibility and robustness.** HDR-4DGS exhibits strong resilience across diverse supervision settings. While both HDR-4DGS and HDR-HexPlane benefit from joint LDR-HDR supervision, HDR-4DGS maintains competitive performance even with LDR-only supervision. This highlights the ability of our dynamic tone mapper and radiance context learner to extract and exploit temporal radiance correlations, enabling accurate HDR reconstruction even without HDR labels.

**(IV) Practical efficiency.** In addition to rendering quality, HDR-4DGS delivers substantial efficiency improvements. It achieves up to  $36\times$  and  $200\times$  faster inference compared to HDR-HexPlane while preserving competitive training times on HDR-4D-Syn and HDR-4D-Real, respectively. This efficiency gain is critical for scaling HDR synthesis to real-world, dynamic scenarios where runtime performance is a key constraint. Note that adding HDR supervision leads to faster inference for HDR-4DGS (Row 10 v.s. 11 in Tab. 1 and Tab. 2) since using HDR signal would effectively compress the model, as there is no need for the model to generate redundant Gaussian points to approximate the transformation from LDR to HDR.

Overall, the results confirm that HDR-4DGS sets a new state of the art in HDR DNVS by jointly optimizing HDR fidelity, dynamic tone adaptation, and inference efficiency both on synthetic and real datasets.

## 4.2 QUALITATIVE RESULTS

While PSNR, SSIM, and LPIPS are commonly used metrics, they may not fully capture perceptual quality, necessitating qualitative visual evaluation. As shown in Fig. 2, HDR-HexPlane fails to reconstruct extreme radiance details, while HDR-4DGS successfully captures more intricate structures. From Fig. 3, it can be observed that HDR-GS struggles to reconstruct dynamic objects, and HDR-HexPlane tends to produce over-smoothed results. In contrast, HDR-4DGS effectively represents the dynamic scene while preserving finer details. Meanwhile, temporal radiance consistency is also challenged by HDR-HexPlane, while HDR-4DGS synthesizes spatiotemporally coherent HDR results, as illustrated in Fig. 4. Please refer to Appendix A.2 for more visualization comparisons.

## 4.3 ABLATION STUDY

To validate the effectiveness of the dynamic tone mapper, analyze its architectural design, and determine an appropriate temporal window length as a hyperparameter, we conduct ablation studies on the HDR-4D-Syn dataset.

**Effect of dynamic tone mapper.** To validate our dynamic tone mapper, we conduct comparative experiments against a plain MLP variant, two classical tone mappers Durand (Durand & Dorsey, 2000) and Reinhard (Reinhard et al., 2023) and the static tone mapper adopted by HDR-HexPlane. Additionally, ablation studies are performed to assess the contribution of extra pixel-level supervision (see Sec. 3.4). Key findings are: **(I)** Tab. 3 reveals that when replacing our dynamic tone mapper with other existing counterparts, we observe significant performance degradation. This confirms that explicit modeling of temporal radiance variations through our dynamic tone mapper is critical for maintaining HDR fidelity while existing mappers are inferior in doing that. Further, complementary ablation studies with respect to the scene representation verify that the observed performance gains are primarily attributable to our dynamic tone mapper, rather than 4DGS alone. **(II)** Disabling the pixel-level supervision leads to performance reduction (PSNR decreases by 1.03 dB), as shown in Tab. 4. This demonstrates that joint optimization with both ray-level and pixel-level constraints provides essential supervisory signals for learning physically plausible tone mapping operators.

**Design of dynamic radiance context learner.** The temporal radiance variation modeling constitutes a critical component of our dynamic tone mapper, as the temporal coherence of radiance decomposition directly influences HDR rendering performance. To systematically evaluate architectural suitability, we implement the dynamic radiance context learner with multiple sequence models and quantitatively compare their effectiveness. As shown in Tab. 5, while Transformer-based modules demonstrate theoretical advantages in long-term dependency modeling (Wen et al., 2023), our experiments reveal superior performance when employing GRU. This observation aligns with recent findings in sequence feature extraction, where GRU exhibits better efficiency in capturing local temporal patterns (Li et al., 2023).

Table 3: Ablation on dynamic tone mapping.

| Method                           | PSNR $\uparrow$ | SSIM $\uparrow$ | LPIPS $\downarrow$ |
|----------------------------------|-----------------|-----------------|--------------------|
| Reinhard (Reinhard et al., 2023) | 22.10           | 0.812           | 0.210              |
| Durand (Durand & Dorsey, 2000)   | 22.85           | 0.825           | 0.195              |
| MLP (HDR-GS)                     | 23.92           | 0.841           | 0.142              |
| Ours                             | <b>25.88</b>    | <b>0.865</b>    | <b>0.076</b>       |

Table 4: Analysis of pixel-level supervision.

| Pixel-level Supervision | HDR             |                 |                    |
|-------------------------|-----------------|-----------------|--------------------|
|                         | PSNR $\uparrow$ | SSIM $\uparrow$ | LPIPS $\downarrow$ |
| No                      | 24.85           | 0.853           | 0.169              |
| Yes                     | <b>25.88</b>    | <b>0.865</b>    | <b>0.076</b>       |

In addition, to rigorously evaluate the efficiency of our proposed dynamic tone mapping framework in preserving continuous radiance variations, we conduct ablation studies by substituting our architecture with a plain MLP baseline. Specifically, we synthesize temporally coherent HDR sequences for a dynamic scene using both architectures, with visualization results presented in Figs. 13 - 14 in Appendix A.2. The comparative results show that our HDR-4DGS with dynamic tone mapper achieves superior temporal coherence in radiance transitions compared to baseline approaches, which validates the effectiveness of our dynamic tone mapper.

Table 5: Analysis of DRCL design.

| Network                            | HDR             |                 |                    |
|------------------------------------|-----------------|-----------------|--------------------|
|                                    | PSNR $\uparrow$ | SSIM $\uparrow$ | LPIPS $\downarrow$ |
| RNN (Salehinejad et al., 2017)     | 25.63           | 0.847           | 0.100              |
| LSTM (Staudemeyer & Morris, 2019)  | 25.53           | 0.845           | 0.106              |
| GRU (Cho et al., 2014)             | <b>25.88</b>    | <b>0.865</b>    | <b>0.076</b>       |
| Transformer (Vaswani et al., 2017) | 25.06           | 0.817           | 0.101              |

Table 6: Analysis of the temporal context length.

| Row | $k$ | HDR             |                 |                    |
|-----|-----|-----------------|-----------------|--------------------|
|     |     | PSNR $\uparrow$ | SSIM $\uparrow$ | LPIPS $\downarrow$ |
| 1   | 5   | 24.74           | 0.852           | 0.092              |
| 2   | 10  | 24.76           | 0.851           | 0.098              |
| 3   | 20  | <b>25.88</b>    | <b>0.856</b>    | <b>0.076</b>       |
| 4   | 30  | 24.29           | 0.825           | 0.094              |

**Temporal length.** As described in Sec. 3.3, our dynamic tone mapper extracts radiance cues from the past  $k$  timestamps in the radiance bank using a sliding window and a dynamic radiance context learner. The hyper-parameter  $k$  governs the trade-off between temporal context coverage and computational efficiency: larger  $k$  captures extended radiance dynamics but risk redundancy and noise sensitivity, while smaller  $k$  prioritizes immediate temporal cues at the cost of modeling complex patterns. Through ablation experiments with  $k = 5, 10, 20, 30$ , as shown in Tab. 6, we find that  $k = 20$  achieves optimal performance, balancing responsiveness to dynamic scenes with practical efficiency constraints.

## 5 CONCLUSION

This work introduces the task of High Dynamic Range Dynamic Novel View Synthesis (HDR DNVS), addressing a critical limitation in prior HDR synthesis methods restricted to static scenes. We present HDR-4DGS, a novel framework designed to reconstruct temporally coherent HDR radiance fields and dynamic geometry from sparse, time-varying LDR observations. The key innovation of HDR-4DGS lies in its dynamic tone mapping module, which leverages a radiance bank and a dynamic radiance context learner to drive per-channel tone-mapping functions that adaptively bridge HDR and LDR domains across time. Extensive experiments demonstrate that HDR-4DGS significantly outperforms prior methods in HDR rendering fidelity, temporal radiance consistency, and computational efficiency. Limitations are discussed in Appendix A.3.

## 6 ETHICS STATEMENT

This work is focused on advancing the technical capabilities of dynamic scene reconstruction and HDR rendering from standard LDR video inputs. The proposed method, HDR-4DGS, is intended for research and non-malicious applications such as virtual reality, cinematic content creation, and immersive telepresence.

The synthetic data used in our experiments are generated in controlled simulation environments, and the real-world scenes in our dataset were captured with the informed consent of all participants and property owners. No personally identifiable information is included in the released data. We do not anticipate direct negative societal impacts from this research; however, as with any novel view synthesis technology, potential misuse (*e.g.*, generating misleading visual content) could arise if deployed without appropriate safeguards. We encourage responsible use and advocate for transparency in synthetic media generation.

## 7 REPRODUCIBILITY STATEMENT

We are committed to the reproducibility of HDR-4DGS. The complete code will be publicly released upon final acceptance of this paper. To facilitate verification prior to code release, we provide a thorough description of our method in Sec. 3 and comprehensive implementation details in Sec. 4 and Appendix A.2. Together, these sections cover all essential components of HDR-4DGS, enabling independent replication of our results.

## REFERENCES

- Jad Abou-Chakra, Feras Dayoub, and Niko Sünderhauf. Particlenerf: A particle-based encoding for online neural radiance fields. In *Proceedings of the IEEE/CVF Winter Conference on Applications of Computer Vision*, pp. 5975–5984, 2024.
- Jeongmin Bae, Seoha Kim, Youngsik Yun, Hahyun Lee, Gun Bang, and Youngjung Uh. Per-gaussian embedding-based deformation for deformable 3d gaussian splatting. In *European Conference on Computer Vision*, pp. 321–335. Springer, 2024.
- Yuanhao Cai, Zihao Xiao, Yixun Liang, Minghan Qin, Yulun Zhang, Xiaokang Yang, Yaoyao Liu, and Alan L Yuille. Hdr-gs: Efficient high dynamic range novel view synthesis at 1000x speed via gaussian splatting. *Advances in Neural Information Processing Systems*, 37:68453–68471, 2024.
- Ang Cao and Justin Johnson. Hexplane: A fast representation for dynamic scenes. In *Proceedings of the IEEE/CVF Conference on Computer Vision and Pattern Recognition*, pp. 130–141, 2023.
- Yihang Chen, Qianyi Wu, Weiyao Lin, Mehrtash Harandi, and Jianfei Cai. Hac: Hash-grid assisted context for 3d gaussian splatting compression. In *European Conference on Computer Vision*, pp. 422–438. Springer, 2024.
- Zixuan Chen, Yujin Wang, Xin Cai, Zhiyuan You, Zheming Lu, Fan Zhang, Shi Guo, and Tianfan Xue. Ultrafusion: Ultra high dynamic imaging using exposure fusion. In *Proceedings of the Computer Vision and Pattern Recognition Conference*, pp. 16111–16121, 2025.

- Kyunghyun Cho, Bart van Merriënboer, Dzmitry Bahdanau, and Yoshua Bengio. On the properties of neural machine translation: Encoder–decoder approaches. In *Syntax, Semantics and Structure in Statistical Translation*, pp. 103, 2014.
- Woong Oh Cho, In Cho, Seoha Kim, Jeongmin Bae, Youngjung Uh, and Seon Joo Kim. 4d scaffold gaussian splatting for memory efficient dynamic scene reconstruction. *arXiv preprint arXiv:2411.17044*, 2024.
- Jaeyoung Chung, Jeongtaek Oh, and Kyoung Mu Lee. Depth-regularized optimization for 3d gaussian splatting in few-shot images. In *Proceedings of the IEEE/CVF Conference on Computer Vision and Pattern Recognition*, pp. 811–820, 2024.
- Colin W.G. Clifford, Michael A. Webster, Garrett B. Stanley, Alan A. Stocker, Adam Kohn, Tatyana O. Sharpee, and Odelia Schwartz. Visual adaptation: Neural, psychological and computational aspects. *Vision Research*, 47(25):3125–3131, 2007. ISSN 0042-6989.
- Kangle Deng, Andrew Liu, Jun-Yan Zhu, and Deva Ramanan. Depth-supervised nerf: Fewer views and faster training for free. In *Proceedings of the IEEE/CVF Conference on Computer Vision and Pattern Recognition*, pp. 12882–12891, 2022.
- Yuanxing Duan, Fangyin Wei, Qiyu Dai, Yuhang He, Wenzheng Chen, and Baoquan Chen. 4d-rotor gaussian splatting: towards efficient novel view synthesis for dynamic scenes. In *ACM SIGGRAPH 2024 Conference Papers*, pp. 1–11, 2024.
- Fredo Durand and Julie Dorsey. Interactive tone mapping. In *Eurographics Workshop on Rendering Techniques*, pp. 219–230. Springer, 2000.
- Zhiwen Fan, Kevin Wang, Kairun Wen, Zehao Zhu, Dejia Xu, Zhangyang Wang, et al. Lightgaussian: Unbounded 3d gaussian compression with 15x reduction and 200+ fps. *Advances in Neural Information Processing Systems*, 37:140138–140158, 2024.
- Jiemin Fang, Taoran Yi, Xinggang Wang, Lingxi Xie, Xiaopeng Zhang, Wenyu Liu, Matthias Nießner, and Qi Tian. Fast dynamic radiance fields with time-aware neural voxels. In *SIGGRAPH Asia 2022 Conference Papers*, pp. 1–9, 2022.
- Sara Fridovich-Keil, Giacomo Meanti, Frederik Rahbæk Warburg, Benjamin Recht, and Angjoo Kanazawa. K-planes: Explicit radiance fields in space, time, and appearance. In *Proceedings of the IEEE/CVF Conference on Computer Vision and Pattern Recognition*, pp. 12479–12488, 2023.
- Chen Gao, Ayush Saraf, Johannes Kopf, and Jia-Bin Huang. Dynamic view synthesis from dynamic monocular video. In *Proceedings of the IEEE/CVF International Conference on Computer Vision*, pp. 5712–5721, 2021.
- Kyle Gao, Yina Gao, Hongjie He, Dening Lu, Linlin Xu, and Jonathan Li. Nerf: Neural radiance field in 3d vision, a comprehensive review. *arXiv preprint arXiv:2210.00379*, 2022.
- HDRsoft Team. Photomatrix pro, 2025. URL <https://www.hdrsoft.com/>.
- Xin Huang, Qi Zhang, Ying Feng, Hongdong Li, Xuan Wang, and Qing Wang. Hdr-nerf: High dynamic range neural radiance fields. In *Proceedings of the IEEE/CVF Conference on Computer Vision and Pattern Recognition*, pp. 18398–18408, 2022.
- Lei Jiang. *View transformation and novel view synthesis based on deep learning*. PhD thesis, Loughborough University, 2023.
- Bernhard Kerbl, Georgios Kopanas, Thomas Leimkühler, and George Drettakis. 3d gaussian splatting for real-time radiance field rendering. *ACM Trans. Graph.*, 42(4):139–1, 2023.
- Agelos Kratimenos, Jiahui Lei, and Kostas Daniilidis. Dynmf: Neural motion factorization for real-time dynamic view synthesis with 3d gaussian splatting. In *European Conference on Computer Vision*, pp. 252–269. Springer, 2024.
- Pou-Chun Kung, Seth Isaacson, Ram Vasudevan, and Katherine A. Skinner. Sad-gs: Shape-aligned depth-supervised gaussian splatting. In *Proceedings of the IEEE/CVF Conference on Computer Vision and Pattern Recognition Workshops*, pp. 2842–2851, June 2024.

- Ang Li, Jichun Li, Qing Lin, Chenxi Ma, and Bo Yan. Deep image quality assessment driven single image deblurring. In *2020 IEEE International Conference on Multimedia and Expo (ICME)*, pp. 1–6. IEEE Computer Society, 2020.
- Jiahe Li, Jiawei Zhang, Xiao Bai, Jin Zheng, Xin Ning, Jun Zhou, and Lin Gu. Dngaussian: Optimizing sparse-view 3d gaussian radiance fields with global-local depth normalization. In *Proceedings of the IEEE/CVF Conference on Computer Vision and Pattern Recognition*, pp. 20775–20785, 2024.
- Tianye Li, Mira Slavcheva, Michael Zollhoefer, Simon Green, Christoph Lassner, Changil Kim, Tanner Schmidt, Steven Lovegrove, Michael Goesele, Richard Newcombe, et al. Neural 3d video synthesis from multi-view video. In *Proceedings of the IEEE/CVF Conference on Computer Vision and Pattern Recognition*, pp. 5521–5531, 2022.
- Zhenyu Li, Zehui Chen, Xianming Liu, and Junjun Jiang. Depthformer: Exploiting long-range correlation and local information for accurate monocular depth estimation. *Machine Intelligence Research*, 20(6):837–854, 2023.
- Zhihao Liang, Qi Zhang, Wenbo Hu, Lei Zhu, Ying Feng, and Kui Jia. Analytic-splatting: Anti-aliased 3d gaussian splatting via analytic integration. In *European Conference on Computer Vision*, pp. 281–297. Springer, 2024.
- Jinfeng Liu, Lingtong Kong, Bo Li, and Dan Xu. Gausshdr: High dynamic range gaussian splatting via learning unified 3d and 2d local tone mapping. In *Proceedings of the IEEE/CVF Conference on Computer Vision and Pattern Recognition*, 2025.
- Tao Lu, Mulin Yu, Linning Xu, Yuanbo Xiangli, Limin Wang, Dahua Lin, and Bo Dai. Scaffold-gs: Structured 3d gaussians for view-adaptive rendering. In *Proceedings of the IEEE/CVF Conference on Computer Vision and Pattern Recognition*, pp. 20654–20664, 2024.
- Jie Luo, Tianlun Huang, Weijun Wang, and Wei Feng. A review of recent advances in 3d gaussian splatting for optimization and reconstruction. *Image and Vision Computing*, pp. 105304, 2024.
- Ben Mildenhall, Pratul P Srinivasan, Matthew Tancik, Jonathan T Barron, Ravi Ramamoorthi, and Ren Ng. Nerf: Representing scenes as neural radiance fields for view synthesis. *Communications of the ACM*, 65(1):99–106, 2021.
- Simon Niedermayr, Josef Stumpfegger, and Rüdiger Westermann. Compressed 3d gaussian splatting for accelerated novel view synthesis. In *Proceedings of the IEEE/CVF Conference on Computer Vision and Pattern Recognition*, pp. 10349–10358, 2024.
- Jim Nilsson and Tomas Akenine-Möller. Understanding ssim. *arXiv preprint arXiv:2006.13846*, 2020.
- Albert Pumarola, Enric Corona, Gerard Pons-Moll, and Francesc Moreno-Noguer. D-nerf: Neural radiance fields for dynamic scenes. In *Proceedings of the IEEE/CVF Conference on Computer Vision and Pattern Recognition*, pp. 10318–10327, 2021.
- Erik Reinhard. *High Dynamic Range Imaging*, pp. 1–6. Springer International Publishing, Cham, 2020.
- Erik Reinhard, Michael Stark, Peter Shirley, and James Ferwerda. *Photographic Tone Reproduction for Digital Images*. Association for Computing Machinery, 1 edition, 2023.
- Barbara Roessle, Jonathan T. Barron, Ben Mildenhall, Pratul P. Srinivasan, and Matthias Nießner. Dense depth priors for neural radiance fields from sparse input views. In *Proceedings of the IEEE/CVF Conference on Computer Vision and Pattern Recognition*, pp. 12892–12901, June 2022.
- Hojjat Salehinejad, Sharan Sankar, Joseph Barfett, Errol Colak, and Shahrokh Valaee. Recent advances in recurrent neural networks. *arXiv preprint arXiv:1801.01078*, 2017.
- Johannes L Schonberger and Jan-Michael Frahm. Structure-from-motion revisited. In *Proceedings of the IEEE Conference on Computer Vision and Pattern Recognition*, pp. 4104–4113, 2016.

- Jiwei Shan, Zeyu Cai, Cheng-Tai Hsieh, Shing Shin Cheng, and Hesheng Wang. Deformable gaussian splatting for efficient and high-fidelity reconstruction of surgical scenes. *arXiv preprint arXiv:2501.01101*, 2025.
- Liangchen Song, Anpei Chen, Zhong Li, Zhang Chen, Lele Chen, Junsong Yuan, Yi Xu, and Andreas Geiger. Nerfplayer: A streamable dynamic scene representation with decomposed neural radiance fields. *IEEE Transactions on Visualization and Computer Graphics*, 29(5):2732–2742, 2023.
- Ralf C. Staudemeyer and Eric Rothstein Morris. Understanding lstm – a tutorial into long short-term memory recurrent neural networks, 2019.
- Fengrui Tian, Shaoyi Du, and Yueqi Duan. Mononerf: Learning a generalizable dynamic radiance field from monocular videos. In *Proceedings of the IEEE/CVF International Conference on Computer Vision*, pp. 17903–17913, 2023.
- Ashish Vaswani, Noam Shazeer, Niki Parmar, Jakob Uszkoreit, Llion Jones, Aidan N Gomez, Łukasz Kaiser, and Illia Polosukhin. Attention is all you need. *Advances in Neural Information Processing Systems*, 30, 2017.
- Feng Wang, Sinan Tan, Xinghang Li, Zeyue Tian, Yafei Song, and Huaping Liu. Mixed neural voxels for fast multi-view video synthesis. In *Proceedings of the IEEE/CVF International Conference on Computer Vision*, pp. 19706–19716, 2023.
- Qitai Wang, Lue Fan, Yuqi Wang, Yuntao Chen, and Zhaoxiang Zhang. Freevs: Generative view synthesis on free driving trajectory. *arXiv preprint arXiv:2410.18079*, 2024a.
- Xiang Wang, Chen Wang, Bing Liu, Xiaoqing Zhou, Liang Zhang, Jin Zheng, and Xiao Bai. Multi-view stereo in the deep learning era: A comprehensive review. *Displays*, 70:102102, 2021.
- Yufei Wang, Zhihao Li, Lanqing Guo, Wenhan Yang, Alex Kot, and Bihan Wen. Contextgs: Compact 3d gaussian splatting with anchor level context model. *Advances in Neural Information Processing Systems*, 37:51532–51551, 2024b.
- Yi Wei, Shaohui Liu, Yongming Rao, Wang Zhao, Jiwen Lu, and Jie Zhou. Nerfingmvs: Guided optimization of neural radiance fields for indoor multi-view stereo. In *Proceedings of the IEEE/CVF International Conference on Computer Vision*, pp. 5610–5619, 2021.
- Qingsong Wen, Tian Zhou, Chaoli Zhang, Weiqi Chen, Ziqing Ma, Junchi Yan, and Liang Sun. Transformers in time series: a survey. In *Proceedings of the Thirty-Second International Joint Conference on Artificial Intelligence*, 2023.
- Guanjun Wu, Taoran Yi, Jiemin Fang, Wenyu Liu, and Xinggang Wang. Fast high dynamic range radiance fields for dynamic scenes. In *2024 International Conference on 3D Vision (3DV)*, pp. 862–872. IEEE, 2024a.
- Guanjun Wu, Taoran Yi, Jiemin Fang, Lingxi Xie, Xiaopeng Zhang, Wei Wei, Wenyu Liu, Qi Tian, and Xinggang Wang. 4d gaussian splatting for real-time dynamic scene rendering. In *Proceedings of the IEEE/CVF Conference on Computer Vision and Pattern Recognition*, pp. 20310–20320, 2024b.
- Tong Wu, Yu-Jie Yuan, Ling-Xiao Zhang, Jie Yang, Yan-Pei Cao, Ling-Qi Yan, and Lin Gao. Recent advances in 3d gaussian splatting. *Computational Visual Media*, 10(4):613–642, 2024c.
- Qiangeng Xu, Zexiang Xu, Julien Philip, Sai Bi, Zhixin Shu, Kalyan Sunkavalli, and Ulrich Neumann. Point-nerf: Point-based neural radiance fields. In *Proceedings of the IEEE/CVF Conference on Computer Vision and Pattern Recognition*, pp. 5438–5448, 2022.
- Haosen Yang, Chenhao Zhang, Wenqing Wang, Marco Volino, Adrian Hilton, Li Zhang, and Xiatian Zhu. Improving gaussian splatting with localized points management. In *Proceedings of the IEEE/CVF Conference on Computer Vision and Pattern Recognition*, 2025.

Zeyu Yang, Zijie Pan, Xiatian Zhu, Li Zhang, Yu-Gang Jiang, and Philip HS Torr. 4d gaussian splatting: Modeling dynamic scenes with native 4d primitives. *arXiv preprint arXiv:2412.20720*, 2024a.

Zeyu Yang, Hongye Yang, Zijie Pan, and Li Zhang. Real-time photorealistic dynamic scene representation and rendering with 4d gaussian splatting. *International Conference on Learning Representations*, 2024b.

Tinghui Zhou, Richard Tucker, John Flynn, Graham Fyffe, and Noah Snavely. Stereo magnification: Learning view synthesis using multiplane images. *arXiv preprint arXiv:1805.09817*, 2018.

## A APPENDIX

### A.1 DATASETS

This section elaborates on the HDR-4D dataset introduced in this work. As summarized in Tab. 7, the dataset comprises three monocular acquisition configurations (Airplane, Deer, Lego and Tank) where distinct exposure times are applied across viewpoints, and four multi-view stereo configurations (Hook, Jump, Mutant and Standup) characterized by multi-exposure LDR images capture per viewpoint. This design enables comprehensive evaluation of dynamic scene reconstruction under varying lighting conditions and camera setups. Notably, we explicitly use different exposure times rather than exposure value to render multi-exposure images, which enables precise control over radiance sampling intervals, aligning with recent paper conventions. Fig. 5 and Fig. 6 show some example HDR images and LDR images with different exposure times of different scenes.

Table 7: Statistics of HDR-4D-Syn, HDR / LDR means the number of HDR / LDR images.

| Scenes   | Training |     |     | Testing |     |     | Cameras | Resolution | Exposure Time (s) |
|----------|----------|-----|-----|---------|-----|-----|---------|------------|-------------------|
|          | Frames   | HDR | LDR | Frames  | HDR | LDR |         |            |                   |
| Airplane | 280      | 280 | 280 | 70      | 70  | 70  | 1       | 800×800    | 0.125/2/32        |
| Deer     | 80       | 80  | 80  | 20      | 20  | 20  | 1       | 800×800    | 0.125/2/32        |
| Hook     | 28       | 280 | 840 | 4       | 40  | 120 | 10      | 800×800    | 0.125/2/32        |
| Jump     | 21       | 210 | 630 | 3       | 30  | 90  | 10      | 800×800    | 0.125/2/32        |
| Lego     | 240      | 240 | 240 | 60      | 60  | 60  | 1       | 800×800    | 0.125/2/32        |
| Mutant   | 135      | 405 | 405 | 14      | 42  | 42  | 3       | 800×800    | 0.125/2/32        |
| Standup  | 51       | 255 | 765 | 8       | 40  | 120 | 5       | 800×800    | 0.125/2/32        |
| Tank     | 136      | 136 | 136 | 34      | 34  | 34  | 1       | 800×800    | 0.125/2/32        |

Table 8: Statistics of HDR-4D-Real, HDR / LDR means the number of HDR / LDR images.

| Scenes    | Training |     |     | Testing |     |     | Cameras | Resolution | Exposure Time (s) |
|-----------|----------|-----|-----|---------|-----|-----|---------|------------|-------------------|
|           | Frames   | HDR | LDR | Frames  | HDR | LDR |         |            |                   |
| Bed       | 22       | 132 | 317 | 22      | 79  | 79  | 6       | 4032×3024  | 0.004/0.008/0.017 |
| Excavator | 40       | 240 | 576 | 40      | 144 | 144 | 6       | 4032×3024  | 0.002/0.008/0.033 |
| Tank      | 20       | 40  | 96  | 20      | 24  | 24  | 2       | 4032×3024  | 0.007/0.02/0.05   |
| Toys      | 20       | 40  | 96  | 20      | 24  | 24  | 2       | 4032×3024  | 0.008/0.02/0.1    |

### A.2 ADDITIONAL EXPERIMENTS

**Implementation details.** Since Structure-from-Motion (SfM) (Schonberger & Frahm, 2016) struggles to perform reliably on dynamic monocular videos, we adopt different initialization strategies for synthetic and real-world scenes. Specifically, we randomly initialize  $5 \times 10^4$  Gaussians for each synthetic scene, while for real-world scenes, we initialize the Gaussians using a dense reconstructed point cloud and the input images are downsampled by a factor of 4. In both cases, we maintain the same number of training iterations as 4DGS (Yang et al., 2024a). We conducted all the experiments on a single NVIDIA RTX 4090 GPU.

**Additional visualization results.** Fig. 8 and Fig. 9 present additional HDR DNVS rendering results on the HDR-4D-Syn and HDR-4D-Real datasets, respectively. Qualitative comparisons reveal that HDR-4DGS consistently preserves fine structural details and generates visually compelling renderings. In contrast, HDR-HexPlane tends to produce spatially blurred regions, while HDR-GS exhibits significant failure in reconstructing dynamic content, resulting in incomplete renderings.

Similarly, Fig. 10 and Fig. 11 illustrate the LDR DNVS results on the same datasets. HDR-4DGS demonstrates superior color fidelity and detail retention under LDR conditions. Conversely, HDR-HexPlane again suffers from noticeable blurring artifacts, and HDR-GS fails to accurately recover scene chromaticity, further compromising its ability to render dynamic objects with photometric coherence.

Furthermore, accurate rendering of continuous radiance distributions in HDR DNVS is essential for preserving high-fidelity radiance variations across complex lighting conditions, which often occur

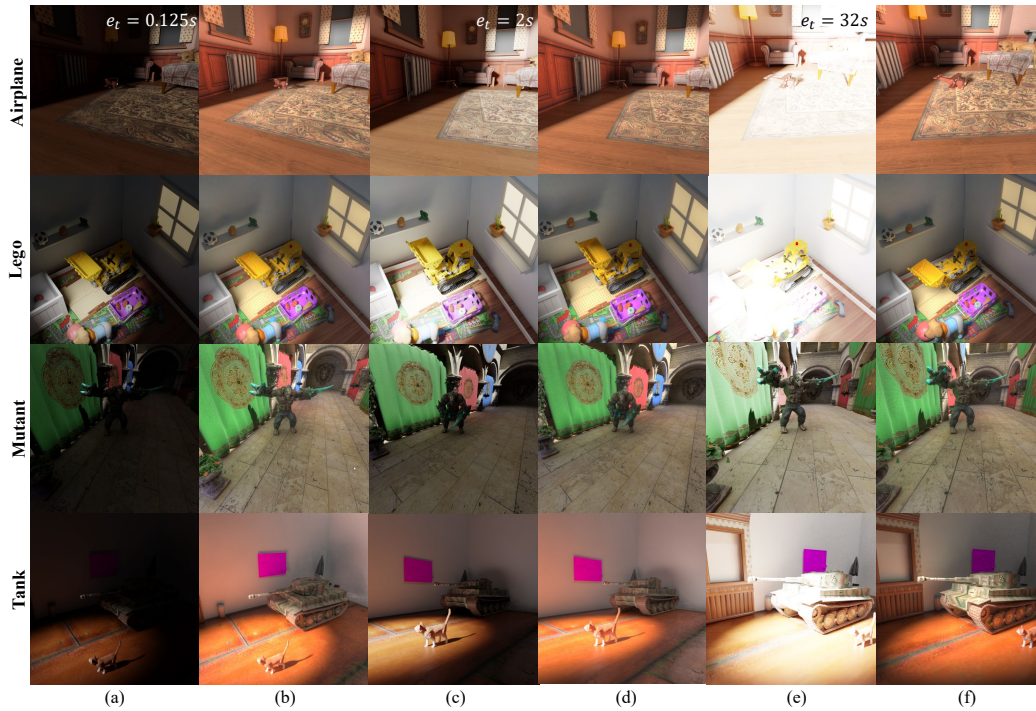


Figure 5: Comparative visualization of LDR and HDR image sequences across dynamic scenes (Airplane, Lego, Mutant, Tank). Each row corresponds to a distinct scene, while columns (a) / (c) / (e) present LDR images captured at varying exposure times and temporal intervals. Columns (b) / (d) / (f) illustrate the HDR counterparts.  $e_t$ : Exposure time.

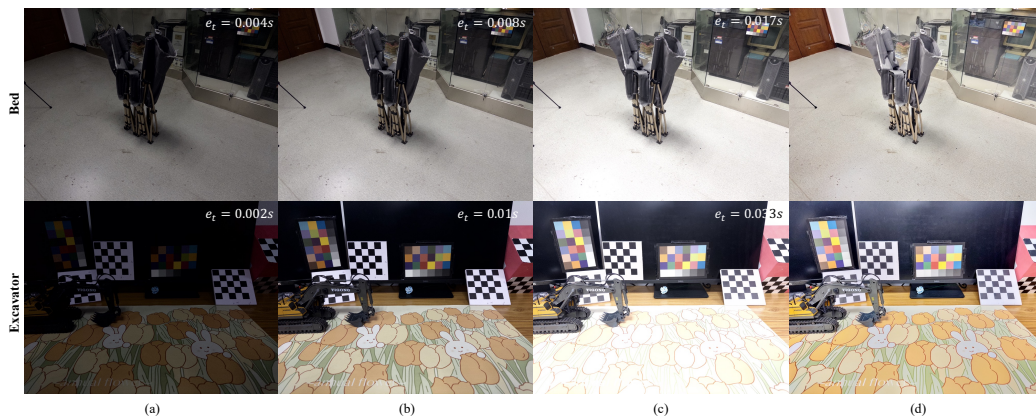


Figure 6: Dataset composition for dynamic scenes (Bed and Excavator) of HDR-4D-Real. Each row corresponds to a distinct scene, with columns (a)–(c) displaying LDR images captured at varying exposure settings but synchronized temporal instances. Column (d) presents the corresponding HDR images at matching temporal frames.  $e_t$ : Exposure time.

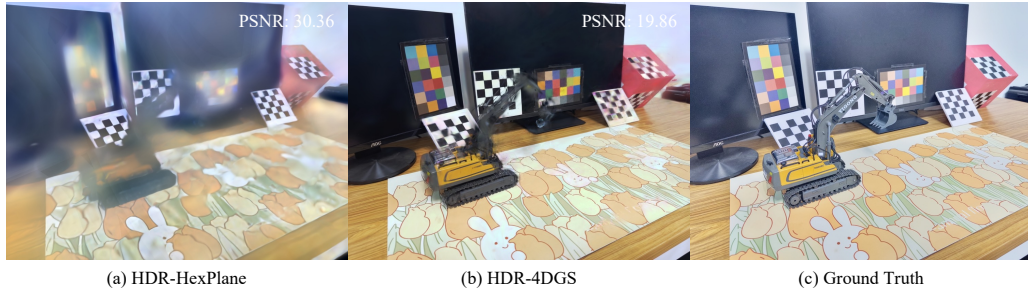


Figure 7: PSNR prefers over-smooth or blurry images. HDR images are tone-mapped by Photomatrix Pro (HDRsoft Team, 2025).

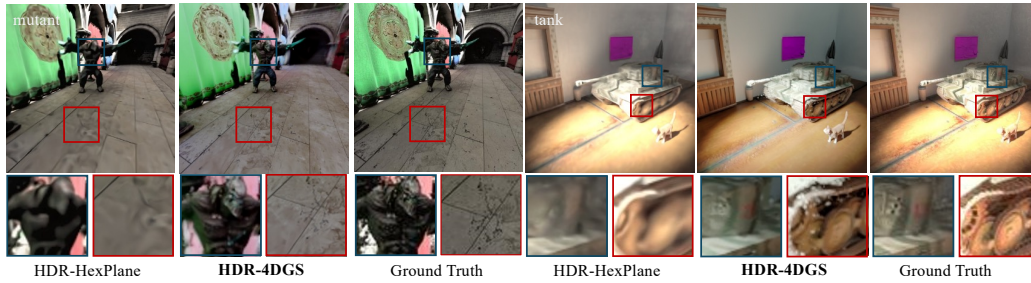


Figure 8: Additional visual comparison of HDR DNVS on HDR-4D-Syn.

in the real-world dynamic scenes. As demonstrated in Fig. 12 and Fig. 13, our HDR-4DGS with dynamic tone mapper featured by a dynamic radiance context learner achieves superior temporal coherence in radiance transitions compared to baseline approaches, effectively capturing smoother details while maintaining photometric consistency. Meanwhile, Fig. 14 provides additional ablation study results of continuous radiance variation comparisons of HDR DNVS, which again, demonstrate the effectiveness of our method.

### A.3 LIMITATIONS

While effective, our approach currently builds upon the existing 4DGS representation, which was not specifically designed for HDR content. A promising direction for future work is to develop a scene representation explicitly tailored to HDR 4D scenes which incorporates physically grounded priors or adaptive radiance bases to better capture extreme illumination variations and enforce long-range temporal coherence. Another key limitation is the use of a fixed temporal context window in our dynamic tone mapper; an adaptive mechanism that modulates the receptive field based on motion magnitude or radiance variance could significantly improve both computational efficiency

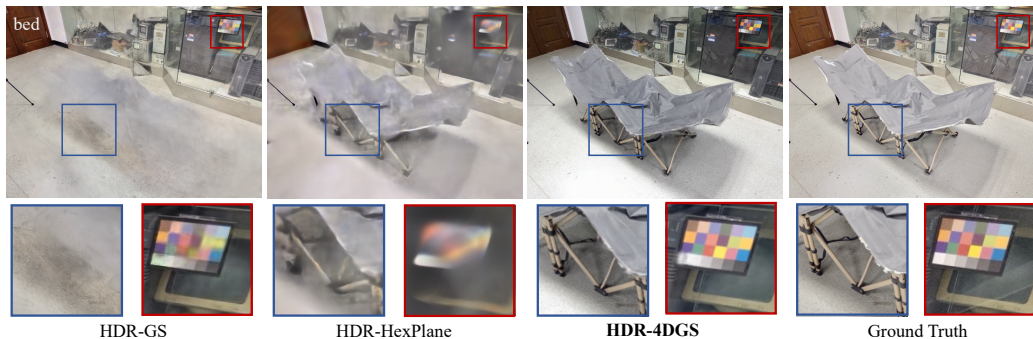


Figure 9: Additional visual comparison of HDR DNVS on HDR-4D-Real.

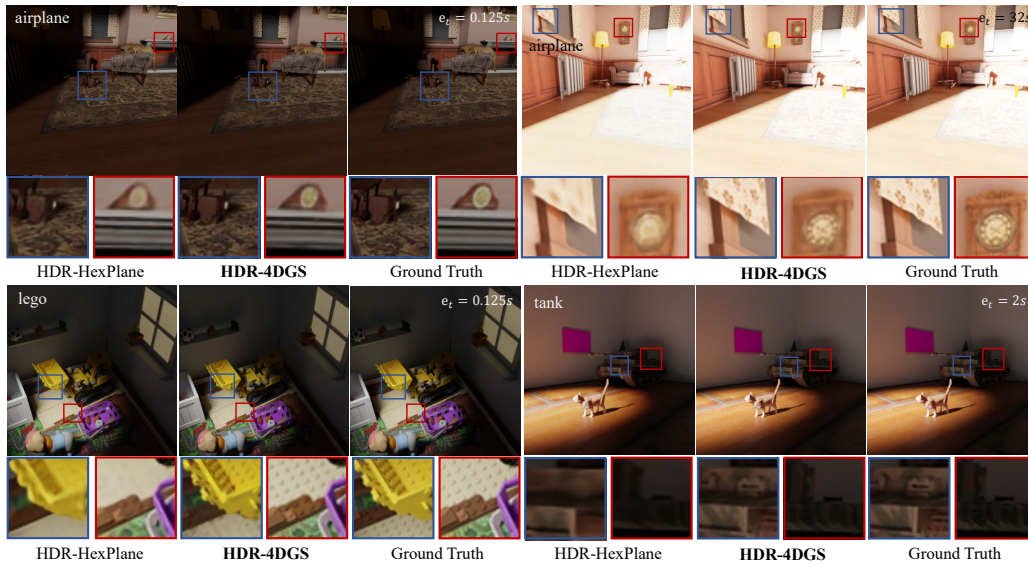


Figure 10: Visual comparison of LDR DNVS on HDR-4D-Syn.

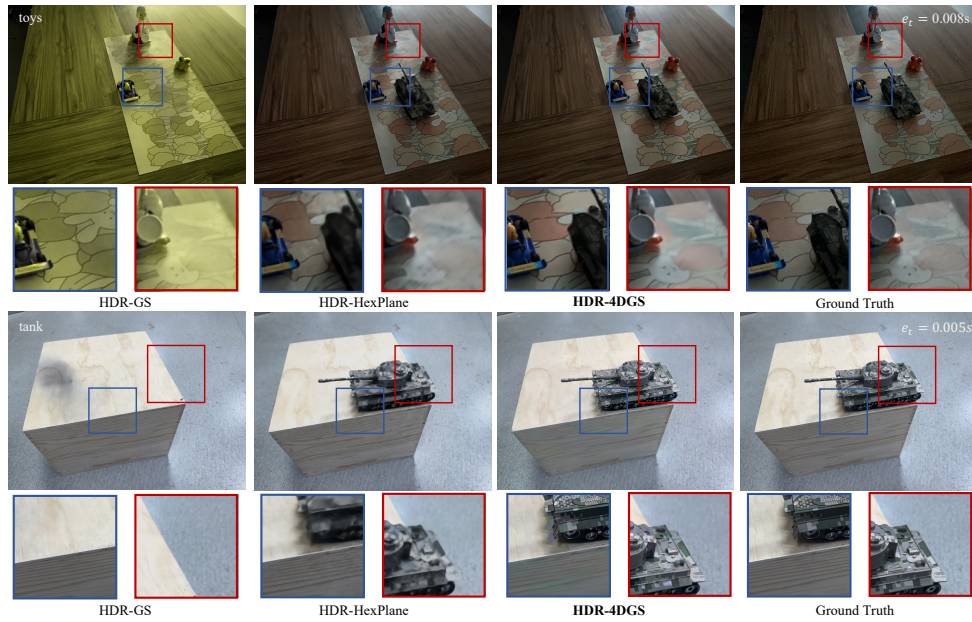


Figure 11: Visual comparison of LDR DNVS on HDR-4D-Real.

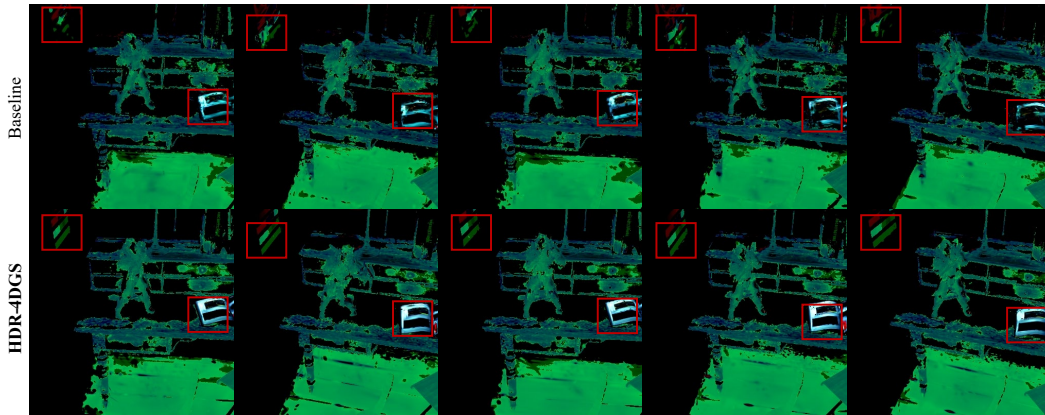


Figure 12: Continuous radiance variations comparison of HDR DNVS. Photomatrix Pro (HDRsoft Team, 2025) is used to facilitate the comparison of radiance transition.

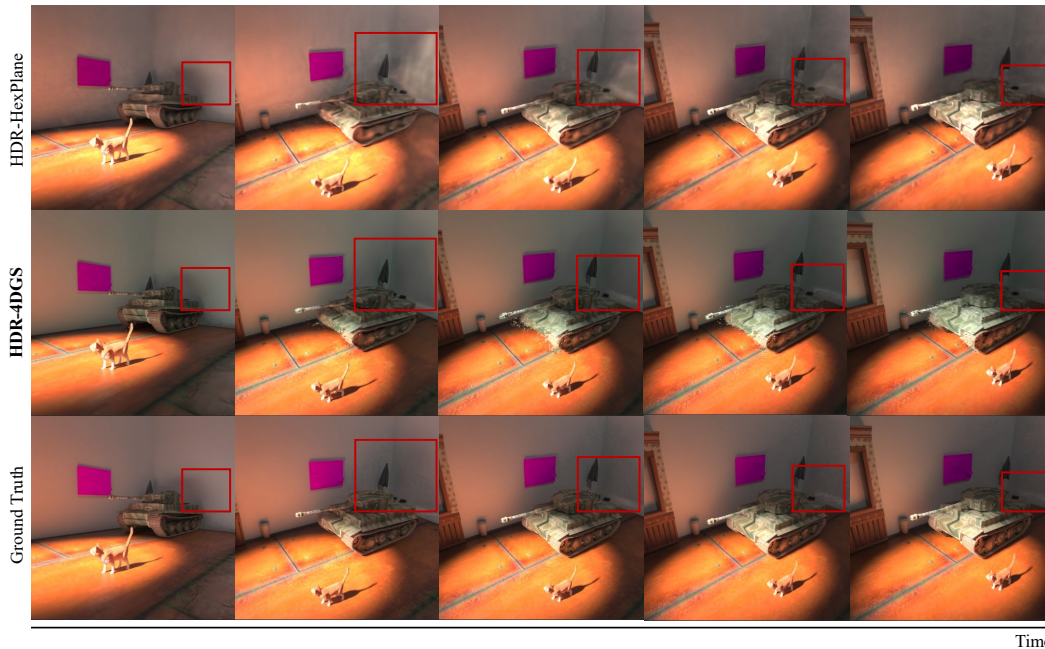


Figure 13: Additional continuous radiance variation comparisons of HDR DNVS on HDR-4D-Syn.

and reconstruction accuracy. Moreover, when foreground and background share similar appearance (*e.g.*, scene jump in HDR-4D-Syn), HDR-4DGS may exhibit suboptimal color reproduction or spatial blurring at dynamic boundaries, suggesting that explicit modeling of semantic or motion boundaries could further disambiguate dynamic content and enhance radiometric consistency across complex scene changes.

#### A.4 THE USAGE OF LARGE LANGUAGE MODELS (LLMs)

We clarify that the use of LLMs in this work is strictly limited to polishing the language and presentation of the manuscript. For instance, the original draft description of our datasets in Sec. 4 read:

“To address the lack of standardized benchmarks for HDR DNVS, we introduce two novel datasets HDR-4D-Syn and HDR-4D-Real. The synthetic dataset, *HDR-4D-Syn*, comprising 8 synthetic dynamic scenes, is based on the dataset proposed by Wu et al. (2024a) and features videos captured

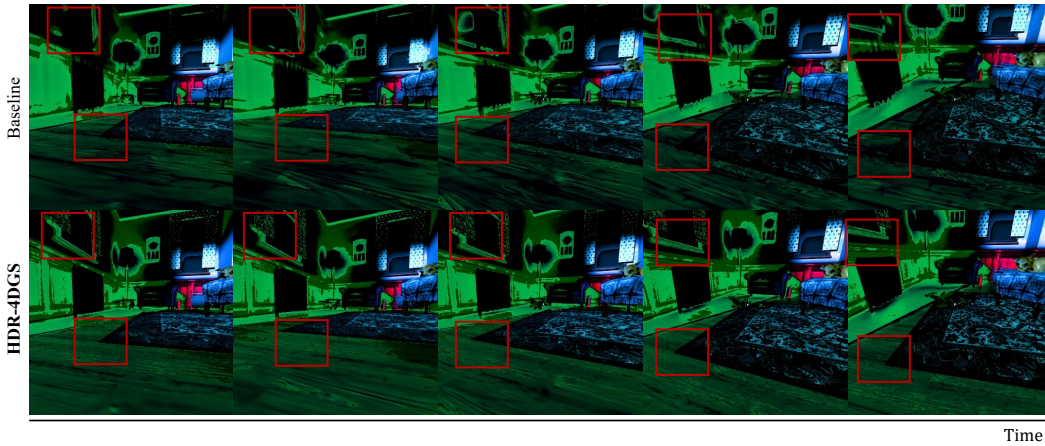


Figure 14: Additional ablation study results of continuous radiance variation comparisons of HDR DNVS on HDR-4D-Syn.

under multi-exposure exposure settings, accompanied by synchronized multi-view LDR video sequences, and corresponding HDR ground truth is re-synthesized. The real-world dataset, *HDR-4D-Real*, consists of 4 real-world indoor dynamic scenes and videos captured under three different exposure times with six iPhone 14 Pro devices, where corresponding HDR images are obtained with UltraFusion (Chen et al., 2025).”

This raw draft was subsequently refined for clarity, grammar, and academic tone — the revised version appearing in the final manuscript reflects only linguistic improvements, with no alteration to technical content or factual claims.